JGR Atmospheres

RESEARCH ARTICLE
10.1029/2022JD036638

Key Points:

- Column formaldehyde (ΩHCHO) is related spatially and temporally with surface ozone during the LISTOS and KORUS-AQ field campaigns
- ΩHCHO better correlates with O_x (≡ozone + NO_2) which more broadly represents ozone and related photochemical oxidants
- Satellite ΩHCHO could be an indicator of ozone and related photochemical oxidants and inform air quality monitoring strategies

Supporting Information:

Supporting Information may be found in the online version of this article.

Correspondence to:

K. R. Travis and L. M. Judd,
katherine.travis@nasa.gov;
laura.m.judd@nasa.gov

Citation:

Travis, K. R., Judd, L. M., Crawford, J. H., Chen, G., Szykman, J., Whitehill, A., et al. (2022). Can column formaldehyde observations inform air quality monitoring strategies for ozone and related photochemical oxidants? *Journal of Geophysical Research: Atmospheres*, *127*, e2022JD036638. https://doi.org/10.1029/2022JD036638

Received 14 FEB 2022
Accepted 4 JUN 2022

Author Contributions:

Conceptualization: K. R. Travis, L. M. Judd, J. H. Crawford
Data curation: Gao Chen, Elena Spinei, Scott Janz, Caroline R. Nowlan, Hyeong-Ahn Kwon, Alan Fried, James Walega
Formal analysis: K. R. Travis, L. M. Judd, J. H. Crawford

Can Column Formaldehyde Observations Inform Air Quality Monitoring Strategies for Ozone and Related Photochemical Oxidants?

K. R. Travis[1], L. M. Judd[1], J. H. Crawford[1], Gao Chen[1], James Szykman[2], Andrew Whitehill[2], Lukas C. Valin[2], Elena Spinei[3], Scott Janz[4], Caroline R. Nowlan[5], Hyeong-Ahn Kwon[6], Alan Fried[7], and James Walega[7]

[1]NASA Langley Research Center, Hampton, VA, USA, [2]Office of Research and Development, United States Environmental Protection Agency, Research Triangle Park, NC, USA, [3]Center for Space Science and Engineering Research, Virginia Polytechnic Institute and State University, Blacksburg, VA, USA, [4]NASA Goddard Space Flight Center, Greenbelt, MD, USA, [5]Atomic and Molecular Physics Division, Harvard–Smithsonian Center for Astrophysics, Cambridge, MA, USA, [6]Department of Environmental and Energy Engineering, The University of Suwon, Gyeonggi-do, Republic of Korea, [7]Institute of Arctic and Alpine Research (INSTAAR) at the University of Colorado, Boulder, CO, USA

Abstract Formaldehyde column density (ΩHCHO) showed a potentially useful correlation with surface ozone during the LISTOS campaign on Long Island Sound and the KORUS-AQ campaign in Seoul, South Korea. This builds on previous work that identified this relationship from in situ aircraft observations with similar findings for ground-based and airborne remote sensing of ΩHCHO. In the Long Island Sound region, ΩHCHO and surface ozone exhibited strong temporal ($r^2 = 0.66$) and spatial ($r^2 = 0.73$) correlation. The temporal variability in ΩHCHO (~1 Dobson units [DU]) was larger than the range in the spatial average (~0.1 DU). The spatial average is most useful for informing ozone monitoring strategies, demonstrating the challenge in using ΩHCHO satellite data sets for this purpose. In Seoul, high levels of NO_2 resulted in O_x better correlating with ΩHCHO than surface ozone due to titration effects. The ΩHCHO–O_x relationship may therefore reflect the sum of surface ozone and related photochemical oxidants, relevant to air quality standards set to regulate this quantity such as the U.S. EPA National Ambient Air Quality Standard (NAAQS). The relationship of ΩHCHO to O_x shifted in Seoul during the campaign demonstrating the need to evaluate this relationship over longer time periods. With sufficient precision in future satellite retrievals, ΩHCHO observations could be useful for evaluating the adequacy of surface air quality monitoring strategies.

Plain Language Summary Surface ozone is hazardous to human health and the environment. Space-based monitoring techniques provide the opportunity to improve our knowledge of regional surface ozone pollution. Ozone measurements from space have limited ability to detect surface concentrations. Observations of column formaldehyde, a trace gas produced during production of surface ozone, are correlated with surface ozone and related pollutants. This relationship points to a potential use of satellite observations for identifying regions of harmful ozone concentrations to complement sparse surface monitoring networks.

1. Introduction

Surface ozone continues to exceed recommended air quality standards created to protect human health and the environment in many regions of the world (Cooper et al., 2014; Gaudel et al., 2018). Monitoring ozone levels to assess exposure and inform efforts to adhere to these standards is challenged by sparse surface networks and limited sensitivity of satellite sensors to the lower troposphere (Costantino et al., 2017; Gonzalez Abad et al., 2019). The use of satellite information to inform ozone air quality has largely been confined to observations of ozone precursors such as nitrogen dioxide (NO_2) and formaldehyde (HCHO). Tonnesen and Dennis (2000) first proposed that in situ HCHO/NO_2 was a useful metric for ground-level ozone sensitivity (NO_x- vs. volatile organic compound [VOC]-limited), particularly when conditions were removed from the transition between those two regimes. The ratio of column HCHO/NO_2 from satellite retrievals has been applied in a similar manner (Duncan et al., 2010; Jin & Holloway, 2015; Jin et al., 2020; Martin et al., 2004) but is subject to additional ambiguity due to differences in the vertical distribution of HCHO versus NO_2 (Schroeder et al., 2017).

Methodology: K. R. Travis, L. M. Judd, J. H. Crawford
Software: K. R. Travis, L. M. Judd
Visualization: K. R. Travis, L. M. Judd
Writing – original draft: K. R. Travis, L. M. Judd, J. H. Crawford
Writing – review & editing: K. R. Travis, L. M. Judd, J. H. Crawford, Gao Chen, James Szykman, Andrew Whitehill, Lukas C. Valin, Elena Spinei, Scott Janz, Caroline R. Nowlan, Hyeong-Ahn Kwon, Alan Fried

During the DISCOVER-AQ campaign, designed for improving the interpretation of satellite air quality data in four polluted regions of the United States, Schroeder et al. (2016) found a strong relationship between surface ozone and HCHO column density (ΩHCHO) derived from in situ aircraft observations. HCHO and ozone are coproduced through the photochemical oxidation of VOCs in the presence of NO_x. The short lifetime of HCHO (several hours) results in a close correlation between the column amount, largely confined to the surface mixed layer, and surface photochemistry. This relationship motivates exploring the use of ΩHCHO to identify areas of unhealthy surface ozone in polluted regions to identify gaps in air quality monitoring efforts.

Pollution monitoring from space is entering a transitional period with the emergence of hourly observations at higher spatial resolution (<10 km) with the launch of geostationary satellite sensors beginning with GEMS (Geostationary Environment Monitoring Spectrometer) over East Asia in 2020 (Kim et al., 2020) that will be followed by TEMPO (Tropospheric Emissions: Monitoring of POllution) over the United States in 2022 (Zoogman et al., 2017), and Sentinel-4 over Europe and northern Africa soon after (Ingmann et al., 2012). These satellite trace gas retrievals will provide an opportunity to better understand air quality at finer scales. In preparation for these emerging satellite observations, recent field studies collected multiperspective data sets from in situ and remote sensing platforms to improve interpretation of temporal and spatial relationships of column-based observations to surface air quality. We take advantage of ΩHCHO observations from two recent campaigns, the Long Island Sound Tropospheric Ozone Study (LISTOS) and Korea–United States Air Quality (KORUS-AQ) study to further investigate the relationship between ΩHCHO and surface ozone identified during DISCOVER-AQ.

2. Description of LISTOS and KORUS-AQ Observations

Relevant details about ΩHCHO and surface trace gas observations used in this analysis from LISTOS and KORUS-AQ are briefly described below and summarized in Table 1.

2.1. Long Island Sound Tropospheric Ozone Study

LISTOS was a multiagency collaborative air quality study conducted in the vicinity of Long Island Sound in summer 2018. The region is currently in moderate nonattainment of the ozone National Ambient Air Quality Standard (NAAQS, U.S. EPA, 2021). The study investigated the lack of improved ozone design values along the region's shoreline despite emissions reductions over the last few decades (NESCAUM, 2017). A primary goal of LISTOS was to better understand the features of ozone production and transport downwind of New York City over Long Island Sound that are responsible for exceedances of the 8-hr ozone NAAQS. Observations included airborne in situ and remote sensing platforms, and ground measurements of ozone and its precursors (Karambelas, 2020).

The LISTOS study produced a robust data set of repeated raster mapping of ΩHCHO with the NASA Geostationary Trace gas and Aerosol Sensor Optimization (GeoTASO, Leitch et al., 2014) on the NASA LaRC HU-25 aircraft in late June 2018 and the GEO-CAPE Airborne Simulator (GCAS, Kowalewski & Janz, 2014) on the NASA LaRC B200 from July through September 2018. Differences between GeoTASO and GCAS are small and are described, along with the flight strategies, in Judd et al. (2020). All references to either instrument will herein be referred to as "airborne spectrometer." Airborne spectrometer ΩHCHO observations are available for during 26 flights on 13 flight days (primarily between 8:00 and 17:00 LT) from 25 June to 6 September 2018 (Janz et al., 2019; Judd et al., 2020). A retrieval description is provided in Janz et al. (2019) with further details in Section S1 in Supporting Information S1. For this analysis, the airborne ΩHCHO observations are compared to hourly surface ozone from 22 State and Local Air Monitoring Stations (SLAMS) that report to the EPA Air Quality System (AQS) in the study domain. Preliminary analysis (not shown) revealed that early morning observations (<10 LT), prior to significant photochemical activity, do not show a strong relationship between ΩHCHO and surface ozone. Therefore, data collected before 10 LT are not considered in this analysis. To provide context on how flight days compare to all days in this time period, a timeseries of daytime (10–16 LT) average surface ozone from the 22 SLAMS sites overlaid by the ozone corresponding to the airborne spectrometer coincidences on the 13 flight days is provided in Figure S1 in Supporting Information S1.

Table 1
Summary of Measurements and Comparison Criteria for KORUS-AQ and LISTOS Data Sets

ΩHCHO instrument	ΩHCHO sampling details	Ozone and NO_2 surface measurements
LISTOS		
Airborne spectrometer (GCAS/GeoTASO)	• Onboard the NASA LaRC B-200 (July–September 2018) or HU-25 (June 2018) • 26 flights on 13 flight days • Primarily between 8 and 17 LT and averaged within a 1 km radius of SLAMS sites for comparison	• Surface ozone from 22 SLAMS and NO_2 from 9 SLAMS • Compared to the nearest 1 hr of the aircraft overpass
KORUS-AQ		
Airborne spectrometer (GeoTASO)	• Onboard the NASA LaRC B-200 • 27 flights over 17 flight days • ΩHCHO retrieved over Olympic Park 25 times between 10 and 18 LT and averaged within a 1 km radius for comparison	• AirKorea ozone and NO_2 at Olympic Park • Averaged within ±0.5 hr window from the aircraft overpass
Airborne in situ mid-IR absorption spectrometer	• Onboard the NASA DC-8 • 1-Hz data integrated into ΩHCHO as described in Section S2 in Supporting Information S1 • 33 descents over Olympic Park after 10 LT	• Seven AirKorea sites along the flight path with ozone and NO_2 • Averaged over a ±0.5-hr window from the aircraft overpass
Pandora spectrometer	• Located at Olympic Park • Direct-sun mode, 4937 ~90 s observations with uncertainty <0.25 DU	• AirKorea ozone and NO_2 at Olympic Park • Matched within 5 min or less

2.2. Korea–United States Air Quality Study

The KORUS-AQ field study took place from 2 May to 10 June 2016. The campaign overview is provided in Crawford et al. (2021). We focus on three ΩHCHO measurements at or near the Olympic Park ground site (37.5216°N, 127.1242°E) that include (a) in situ profiles from the NASA DC-8, (b) a Pandora spectrometer, and (c) airborne spectrometer (GeoTASO) overflights. This analysis aims to intercompare these measurements and investigate their relationship to surface ozone from the AirKorea regulatory monitoring network in the vicinity of Olympic Park.

The airborne spectrometer was onboard the NASA LaRC B-200 aircraft and flew 27 flights over 17 flight days. Unlike the LISTOS campaign, flights only included a small subset of raster-like patterns. As a result, observations lacked sufficient measurement density to investigate the ΩHCHO–ozone relationship across a large region as was done for LISTOS. Instead, observations were concentrated over the vicinity of the Olympic Park site in the Seoul Metropolitan Area (SMA). This site also included Pandora observations, nearby surface AirKorea monitors, and frequent in situ profiling by the NASA DC-8. ΩHCHO was retrieved from the airborne spectrometer over Olympic Park 25 times between 10 and 18 LT. The airborne spectrometer ΩHCHO retrieval is described in Kwon et al. (2021).

The DC-8 aircraft was equipped with an onboard 1 Hz in situ HCHO instrument (Fried et al., 2020). This instrument, a mid-IR absorption spectrometer, acquired HCHO measurements during frequent descents ($n = 33$ after 10 LT) over the Olympic Park site, constrained at the surface with a ground HCHO measurement run by the U.S. EPA (Spinei et al., 2018) to provide in situ derived ΩHCHO (detailed calculation in Section S2 in Supporting Information S1). The EPA also operated a Pandora spectrometer at Olympic Park in direct-sun mode for continuous observations of ΩHCHO (Spinei et al., 2018). The ~90 s Pandora observations ($n = 4{,}937$) were colocated with an AirKorea ozone and NO_x monitor. Pandora ΩHCHO has been corrected for known a positive interference from Delrin off-gassing (Spinei et al., 2021) and was filtered for total uncertainty <0.25 Dobson units (DU). A summary of this correction is provided in Section S3 in Supporting Information S1.

3. ΩHCHO Versus Surface Ozone During LISTOS

Figure 1a shows the density of LISTOS airborne spectrometer ΩHCHO observations overlaid by the SLAMS ozone monitor locations in the domain. Between two and four repeated raster maps were collected on 13 flight days with 26 flights for a total of 37 rasters. The flight strategy included sampling of New York City on all

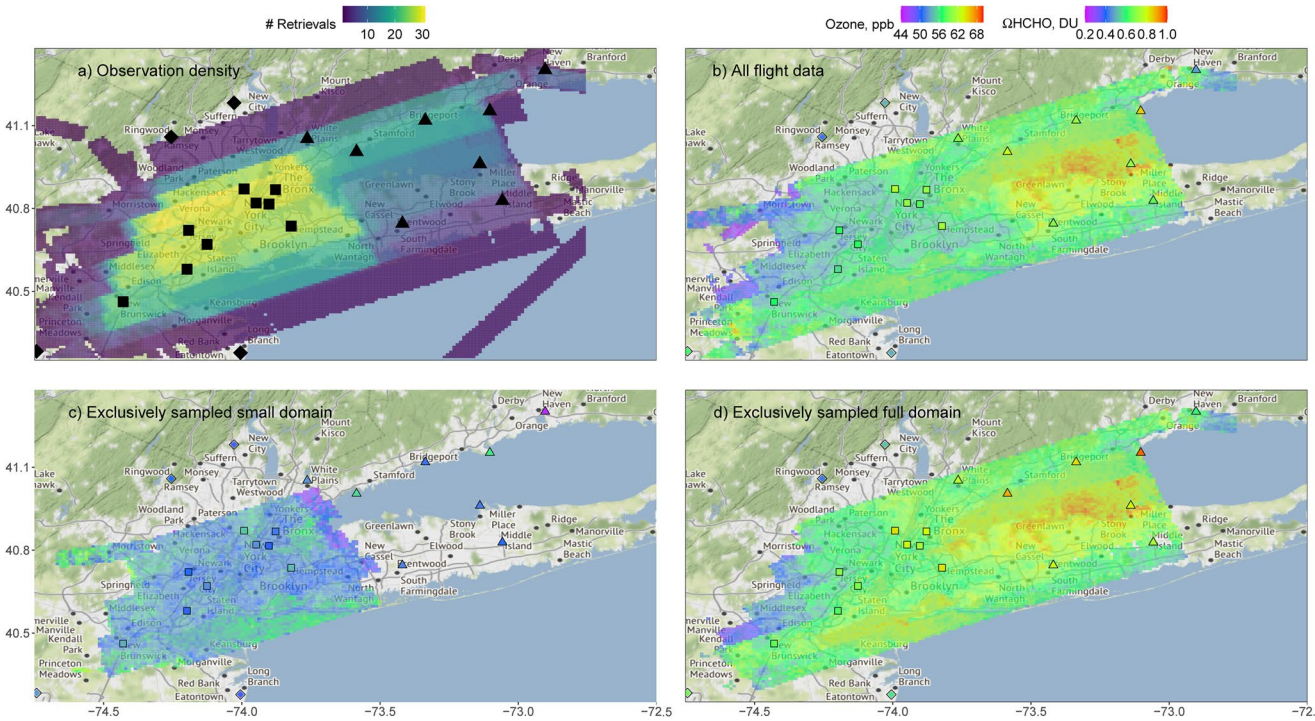

Figure 1. (a) The spatial sampling density of ΩHCHO retrievals collected after 10 LT during LISTOS. Black symbols show the 22 SLAMS ozone monitor locations within the study area. The squares, triangles, and diamonds designate monitors in the small domain, full domain, and outside the domain, respectively. The other three panels show average ΩHCHO with at least five observations during (b) all flight data, (c) flight data for the exclusively sampled small domain, and (d) flight data for the exclusively sampled full domain. The average ozone values between 10 and 16 LT at the SLAMS sites for the days flown are overlaid on each map. The color bar for (b)–(d) is the same. Map tiles by Stamen Design, under CC BY 3.0. Data by © OpenStreetMap contributors, under ODbL.

flight days, with 10 flights expanding further eastward over the full domain, mostly coinciding with high ozone forecasts around Long Island Sound. We consider the impact of this variable sampling strategy to ensure that the relationship between ΩHCHO and surface ozone is not due to preferential sampling of the full domain when ozone events were forecasted.

We define four groupings of the data based on the different airborne flight strategies described above.

1. *All flight data*: 13 flight days/26 flights (37 raster maps) for the entire study region.
2. *Exclusively sampled full domain*: 10 flight days/18 flights (21 raster maps) for the entire study region.
3. *Exclusively sampled small domain*: 5 flight days/8 flights (16 raster maps) for the New York City area.
4. *Small domain*: 13 flight days/26 flights (37 raster maps) for the subset of data over the New York City area.

Figure 1b shows campaign average ΩHCHO for all flight data (excluding areas that had less than 5 ΩHCHO retrievals over the time period of LISTOS). The average ozone mixing ratio for each SLAMS monitor on the flight days between 10 and 16 LT is overlaid. Ozone and ΩHCHO were lowest to the west of New York City with higher values to the east of the domain. However, this is not necessarily representative of actual average conditions since the full domain was not sampled on all flight days. Figures 1c + 1d show average ΩHCHO on flights with exclusive sampling of the small and full domains, respectively. The lower ΩHCHO in the exclusively sampled small domain corresponds to low surface ozone (52 ppb) across the full study domain (all sites in Figure 1c). These relatively cleaner days partially explain the strength of the west-to-east gradient in Figure 1b, highlighting the importance of consistent sampling to observe a true spatial pattern across the domain.

Eighteen flights over 10 days expanded further eastward to map the full domain when forecasts indicated increased ozone over Long Island Sound, resulting in higher regional ozone concentrations (61 ppb). Maximum ozone values occurred at the SLAMS monitors along the Connecticut coast (Figure 1d). The average data collected during flights over the exclusively sampled full domain show an increase in ozone and ΩHCHO from west to east, but this gradient is weaker than for all flight data which includes the cleaner conditions when exclusively

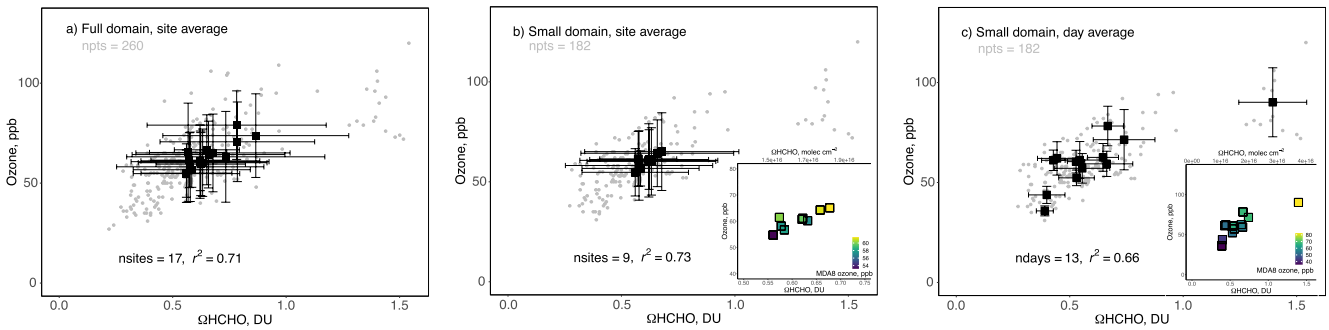

Figure 2. Hourly ozone versus ΩHCHO. Gray points indicate individual coincidences between airborne spectrometer and EPA surface ozone monitors in panels (a)–(c). (a) All flight data with black squares showing site averages and standard deviations. (b) Small domain data with black squares showing site averages and standard deviations. (c) Small domain data with black squares showing daily domain averages and standard deviations. The site averages for a narrower range of ozone and ΩHCHO are shown inset on panel (b) to aid the viewer. This inset shows the site averages colored by average flight day MDA8 ozone. The inset in panel (c) shows the daily domain averages colored by the average MDA8 ozone across the sites. The r^2 values annotated in each panel are for the correlation of the spatially and temporally aggregated points (black squares).

sampling the small domain. The highest ΩHCHO was sampled along the north shore of Long Island (Figures 1b + 1d), but more consistent sampling of ΩHCHO and ozone would be needed to determine whether this is a regular occurrence and indicative of consistently higher ozone or a product of the inconsistent sampling strategy.

Figure 2 investigates the spatial and temporal correlation between ΩHCHO and surface ozone for subsets of the LISTOS data. The aircraft overflew 17 of the 22 SLAMS monitors in the LISTOS study domain at least 5 times (Figure 1a). Figure 2a shows the relationship between ΩHCHO averaged within 1 km of each ground site and the nearest hourly surface ozone for individual coincidences at these sites (gray points, $r^2 = 0.47$). The average of all coincidences for each individual SLAMS site is overlaid (black squares). This demonstrates that ΩHCHO is spatially correlated with ozone in the campaign average ($r^2 = 0.71$). The three sites with average ozone >70 ppb are located downwind of NYC on the coast of Long Island Sound, near Stamford, CT; Bridgeport, CT; and Stony Brook, NY. However, as stated above, all flights did not consistently overfly all 17 SLAMS sites.

Figures 2b + 2c focus on the more frequently sampled nine sites in the small domain (black squares in Figure 1a). The consistent sampling of these sites provides confidence in the strong spatial correlation for site-averaged ΩHCHO and ozone (Figure 2b, $r^2 = 0.73$). The inset panel of Figure 2b shows the site-averaged ΩHCHO and ozone colored by the flight day average maximum daily 8-hr average (MDA8) ozone. As the peak ozone values that drive MDA8 ozone generally occur during similar hours sampled here (10–16 LT), there is a correlation between site average daytime ozone and MDA8 ozone ($r^2 = 0.80$). Thus, elevated ΩHCHO may also be indicative of both elevated daytime and MDA8 ozone. Similarly, when the individual coincidences are averaged for each flight day (Figure 2c), the temporal correlation ($r^2 = 0.66$) and correlation of daily ozone with MDA8 ozone ($r^2 = 0.88$) show that the small domain responds coherently to day-to-day changes in photochemical production of ozone and HCHO.

Ozone and ΩHCHO show greater variability in the daily average (Figure 2c) compared to the site average (Figure 2b). Site average ΩHCHO in the small domain exhibited a range of 0.12 DU (Figure 2b) compared to 1.0 DU in the daily average (Figure 2c). The daily average range in ΩHCHO is reduced to 0.35 DU without the consideration of the day with the highest ΩHCHO that occurred on 2 July. This day was characterized by high temperatures, stagnation, and air mass recirculation (Couillard et al., 2021). The larger daily variability is expected, but the average spatial variability is particularly valuable for informing ozone monitoring strategies. Spatial averaging provides insight as to where higher ΩHCHO, and by extension surface ozone, may occur. Sufficient temporal sampling in this spatial average is important as the ΩHCHO–ozone relationship does not exhibit a consistent spatial pattern from day to day. It is also not well behaved enough to exhibit a one-to-one correspondence useful for predicting ozone at any specific place or time.

When considered individually, all nine sites in the small domain exhibit a statistically significant temporal relationship between ΩHCHO and surface ozone ($r^2 = 0.40$–0.77, p-value <0.05). This implies that a single well-sampled site could be used to establish whether a strong ΩHCHO–ozone relationship is present that could

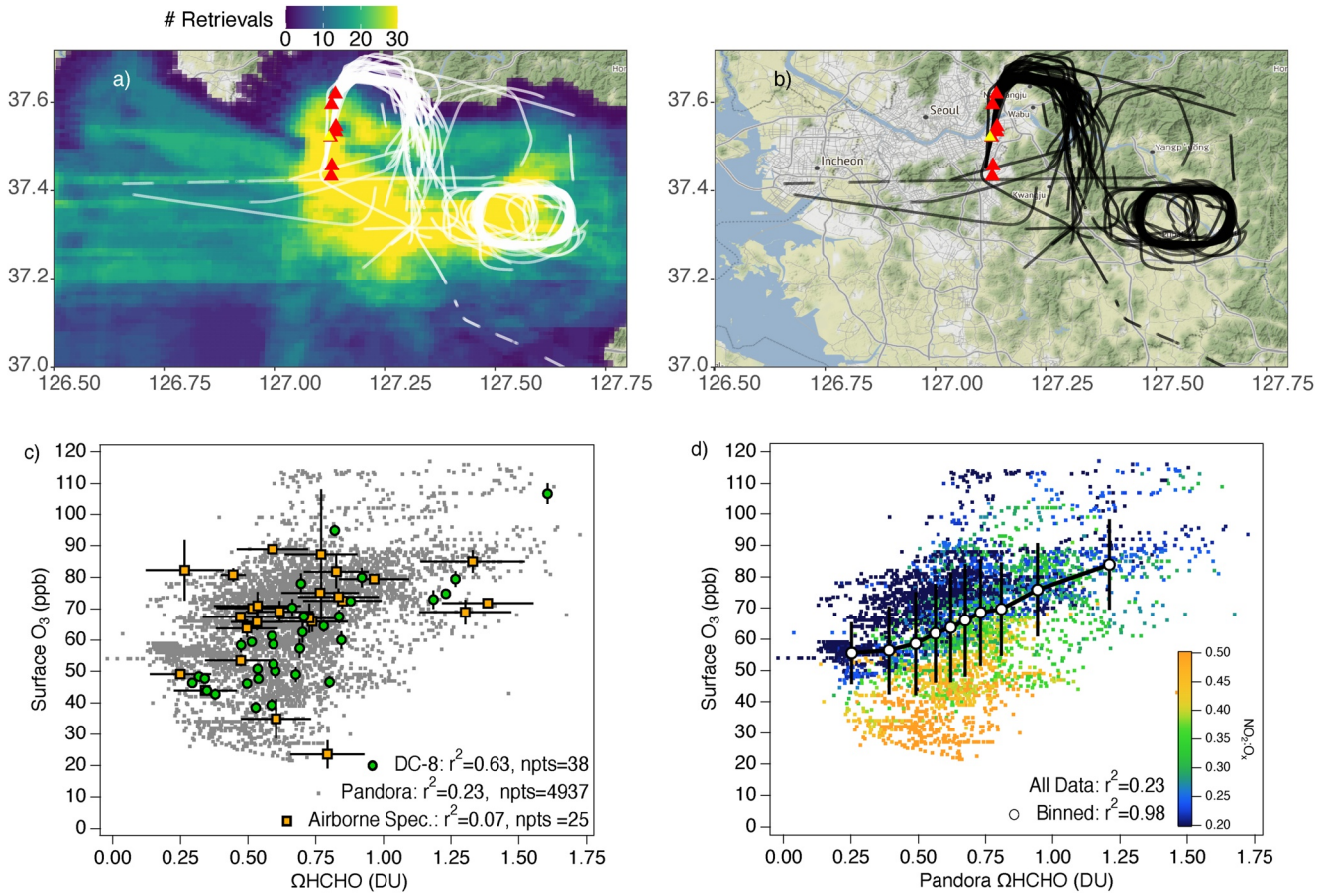

Figure 3. (a) Spatial density of airborne spectrometer ΩHCHO retrievals with DC-8 flight tracks and the seven AirKorea ozone monitors (red triangles) designated along the descent over Olympic Park (yellow triangle). (b) DC-8 flight tracks and AirKorea ozone monitors now overlaid over a map of the SMA. (c) Surface ozone versus ΩHCHO from DC-8 missed approaches (green circles), Pandora (gray dots), and airborne spectrometer (orange squares) at Olympic Park. (d) Surface ozone versus Pandora ΩHCHO colored by NO_2/O_x (discussed in Section 5). Binned data show average ozone and standard deviations for each decile of ΩHCHO (white circles and black lines). Map tiles by Stamen Design, under CC BY 3.0. Data by © OpenStreetMap contributors, under ODbL.

be used to evaluate maps of ΩHCHO for indications of where the greatest ozone impacts are expected across the region.

4. ΩHCHO Versus Surface Ozone During KORUS-AQ From Multiple Perspectives

KORUS-AQ provides a unique opportunity to compare ΩHCHO from multiple perspectives: an airborne remote spectrometer on the B-200 aircraft, in situ profiles from the DC-8 aircraft, and a ground-based Pandora spectrometer at Olympic Park. Figure 3a provides a map of the airborne spectrometer observational density, overlaid by the DC-8 flight tracks for the missed approaches over Olympic Park that were followed by mid-tropospheric to upper tropospheric spirals over Taehwa Research Forest. The DC-8 flight tracks and ground monitor locations are overlaid again on a map of the SMA in Figure 3b. We compare ΩHCHO and surface data sets using these criteria:

1. Pandora and airborne spectrometer ΩHCHO are compared to surface measurements at Olympic Park only and airborne spectrometer data are averaged within a 1 km radius of Olympic Park.
2. DC-8 ΩHCHO are compared to the average of the seven Air Korea monitors along the lowest portion of the aircraft missed approach.
3. Surface monitors are averaged within ±0.5 hr of the ΩHCHO coincidences with the exception of Pandora that is matched to the nearest surface measurement within 5 min. Shorter time windows between ±0.5 hr and ±5 min for averaging surface monitor data do not have a significant impact on the results.

Unlike during LISTOS, airborne spectrometer ΩHCHO shows negligible correlation (r^2 = 0.07) with surface ozone at Olympic Park (Figure 3c). However, DC-8 ΩHCHO shows a strong relationship (r^2 = 0.63). The ΩHCHO–ozone relationship shown in Figure 3c for the 5-min Pandora coincidences (r^2 = 0.23) is also weaker than for the DC-8. However, Pandora ΩHCHO provides a much larger data set to compare to surface ozone (n = 4,937) than for the airborne spectrometer (n = 25) or the DC-8 (n = 33). The average Pandora ΩHCHO total uncertainty (0.05 DU/8%) is smaller than the variability in Figure 3c, thus this lower correlation is likely due to real variability in ΩHCHO and ozone on shorter timescales driven by factors other than photochemistry (i.e., transport). When averaged over decile bins of ΩHCHO (Figure 3d), the relationship between Pandora ΩHCHO and ozone is significantly strengthened (r^2 = 0.98). Therefore, a strong relationship between ΩHCHO and ozone is evident from DC-8 and Pandora observations but not for airborne spectrometer observations. We investigate potential causes for this discrepancy below.

ΩHCHO from the airborne spectrometer, Pandora, and the DC-8 covary with one another, with the best comparison between Pandora and the DC-8 ΩHCHO (Figure S2a in Supporting Information S1; r^2 = 0.80, n = 38). The airborne spectrometer ΩHCHO shows the largest degree of scatter both in comparison to Pandora and DC-8 ΩHCHO (Figures S2b + S2c in Supporting Information S1) and to surface ozone (Figure 3c). We attribute much of this scatter to the higher uncertainty of the airborne spectrometer ΩHCHO, the small sample size, and the impact of outliers.

The DC-8 HCHO observations provide the opportunity to investigate the impact of uncertainties in the a priori HCHO profile used in the airborne spectrometer ΩHCHO retrieval. The largest outlier occurs on 17 May at approximately 17 LT where ozone was high (82 ppb) but ΩHCHO was very low (0.27 DU). During this time, ΩHCHO from the airborne spectrometer is biased low compared to Pandora and DC-8 ΩHCHO (Figure S3a in Supporting Information S1) which is likely due to errors in the a priori profile (Figure S3b in Supporting Information S1). ΩHCHO from the airborne spectrometer increases 37% (from 0.27 to 0.37 DU) when the a priori profile from the DC-8 is used from the previous hour in the air mass factor calculation (Figure S3b in Supporting Information S1), demonstrating the sensitivity of the airborne spectrometer retrieval to errors in this information.

The temporal density of Pandora data provides a method to investigate the impact of the airborne sampling times on the poor correlation with ozone. As shown in Figure S4 in Supporting Information S1, we sample Pandora data only at the times of the airborne spectrometer overpasses and obtain a similarly poor relationship with ozone (r^2 = 0.08, n = 19). If we sample Pandora at the time of the DC-8 overpasses, the relationship is stronger (r^2 = 0.53, n = 22). Unlike airborne spectrometers, Pandora direct-sun retrievals do not require an a priori profile (Spinei et al., 2018). The increased temporal density and lack of dependence on an a priori profile emphasize the value that Pandora provides in building robust statistics to evaluate ΩHCHO–ozone. The expanding network of Pandora spectrometers around the globe will be an asset to help further investigate causes for variability in observed ΩHCHO–ozone relationships. However, only airborne (or space-based) spectrometers can provide regional maps of ΩHCHO that can identify potential areas of elevated ozone. Therefore, improving retrievals of ΩHCHO is imperative to the successful application of this method.

5. The Impact of NO_2 on the ΩHCHO–Ozone Relationship

The relationship between ΩHCHO and ozone can be influenced by NO_x if concentrations are large enough to result in significant ozone titration. To evaluate this impact, we use NO_2 measurements from the SLAMS sites during LISTOS and AirKorea monitors during KORUS-AQ and compare ΩHCHO to O_x, where $O_x = O_3 + NO_2$. Based on the expected interferences from NO_2 oxidation products for the majority of these monitors that continue to use molybdenum oxide converters (Dunlea et al., 2007), these NO_2 levels must be considered an upper limit.

During LISTOS, in situ NO_2 measurements were available for approximately 60% of the airborne spectrometer ΩHCHO and corresponding ozone observations in Figure 2b. For that subset of ozone and NO_2 observations, the relationship remains unchanged when considering ΩHCHO–ozone (r^2 = 0.53) or ΩHCHO–O_x (r^2 = 0.52). With the available data, we conclude that average NO_2 levels were low enough (6 ± 4 ppb between 10 and 18 LST) relative to ozone (59 ± 15 ppb) that the impact of ozone titration was minimal.

During KORUS-AQ, NO_2 and ozone at Olympic Park averaged 27 ± 12 and 66 ± 18 ppb, respectively, during Pandora ΩHCHO coincidences. This results in an average NO_2/O_x fraction of 29%, which is 3 times greater than

observed during LISTOS (9%). Figure 3d shows the Pandora ΩHCHO–ozone data colored by the value of NO_2/O_x. Ozone titration has the greatest impact on the ΩHCHO–ozone relationship for ozone below approximately 40 ppb when NO_2/O_x is highest. High NO_2/O_x also favors lower values of ΩHCHO, which is consistent with the suppression of radicals and the reduced oxidation of VOCs.

Figure 4 explores the effect of ozone titration further by showing Pandora and DC-8 ΩHCHO compared against ozone (a and d), NO_2 (b and e), and O_x (c and f). The ΩHCHO–O_x relationship is stronger than ΩHCHO–ozone for both Pandora ($r^2 = 0.44$ vs. 0.23) and the DC-8 ($r^2 = 0.73$ vs. 0.63). The lowest surface ozone values no longer depart from the relationship with ΩHCHO when viewed as O_x. Pandora (or satellite-based ΩNO_2) can provide an indicator of the presence of high NO_2/O_x if surface NO_2 measurements are unavailable and the correlation of ΩHCHO with surface ozone shows evidence of possible titration (i.e., Figure 3d). This is illustrated by Figure S5 in Supporting Information S1 showing the strong correlation between ΩNO_2 and surface NO_2 ($r^2 = 0.62$).

In South Korea, temperatures increased from May to June in 2016, resulting in higher isoprene emissions and increasing ΩHCHO. The Pandora instrument provides an immense amount of data to look at changes in ΩHCHO–O_x over this transition. The data in Figures 4a–4c are colored by date. ΩHCHO generally increases from the beginning (May) to the end of the campaign (June). Separating the data by month shows that ΩHCHO is larger in June for a given increase in O_x (Figure 4c). The strength of the relationship (r^2) remains largely unchanged as only the ΩHCHO–O_x slope is affected. The decrease in slope does not reflect a decrease in ozone, as average ozone is 65 ppb in May versus 69 ppb in June (Figure 4a). Higher ozone is expected with increasing isoprene emissions in the VOC-limited conditions in Seoul (Schroeder et al., 2020). Instead, the increase in VOCs likely results in greater oxidation of NO_2 to NO_x reservoirs (e.g., peroxyacetylnitrate [PAN]) as reflected by the decrease in NO_2 from May to June (Figure 4b). Figure S6c in Supporting Information S1 shows an increasing trend in average daytime PAN below 0.5 km for the DC-8 aircraft descents over the campaign. An increase in HNO_3 is also observed, but as the aircraft observations do not indicate a clear increase in OH or ozone photolysis frequency over the campaign (Figures S6a + S6b in Supporting Information S1) it is difficult to attribute the cause for this increase.

The shift from May to June in ΩHCHO raises the question of whether the ratio ΩHCHO/ΩNO_2 provides insight into surface ozone pollution. Previous studies have suggested that the ratio ΩHCHO/ΩNO_2 is a useful indicator of surface ozone sensitivity to precursor emissions (i.e., Duncan et al., 2010). This ratio, provided by Pandora, shifts from 0.5 to 0.7 from May to June. These values are indicative of VOC-limited conditions in both months and are outside the range of ambiguity described by Schroeder et al. (2017). However, this metric is of limited value as it fails to consider the impact of NO_x emissions on the footprint of regional ozone production which spans the full range of ozone sensitivity to NO_x and VOC emissions. As a result, ozone will not decrease in the broader region without reductions in NO_x (Schroeder et al., 2020).

In the United States, the ozone NAAQS is in fact defined as a standard for both ozone and related photochemical oxidants, where photochemical oxidants are products of the oxidation of NO in the presence of VOCs (ozone, NO_2, HCHO, PAN, HNO_3, etc.; U.S. EPA, 1978, 2020). The primary indicator for the NAAQS is ozone since it can be measured with high specificity and is easily implemented for widespread monitoring. Thus, the greater sensitivity of ΩHCHO to O_x carries relevance for the larger concern of total photochemical oxidants that ground-based ozone measurements are intended to address. This suggests that areas identified for attention based on ΩHCHO maps could warrant a suite of measurements that include ozone, NO_2, and other photochemical oxidants when possible. In South Korea, NO_x emissions are declining due to local emissions controls. This is expected to lead to initially increasing ozone in the SMA (Schroeder et al., 2020) and ozone will make up a larger fraction of O_x and total photochemical oxidants.

6. Conclusions and Future Directions

The relationship between aircraft in situ derived ΩHCHO and surface ozone identified by Schroeder et al. (2016) suggested the potential for ΩHCHO to improve ozone air quality monitoring strategies from space. We built on this work using remote sensing and in situ derived observations of ΩHCHO available from the 2018 LISTOS campaign in the vicinity of Long Island Sound and the 2016 KORUS-AQ campaign in Seoul, South Korea.

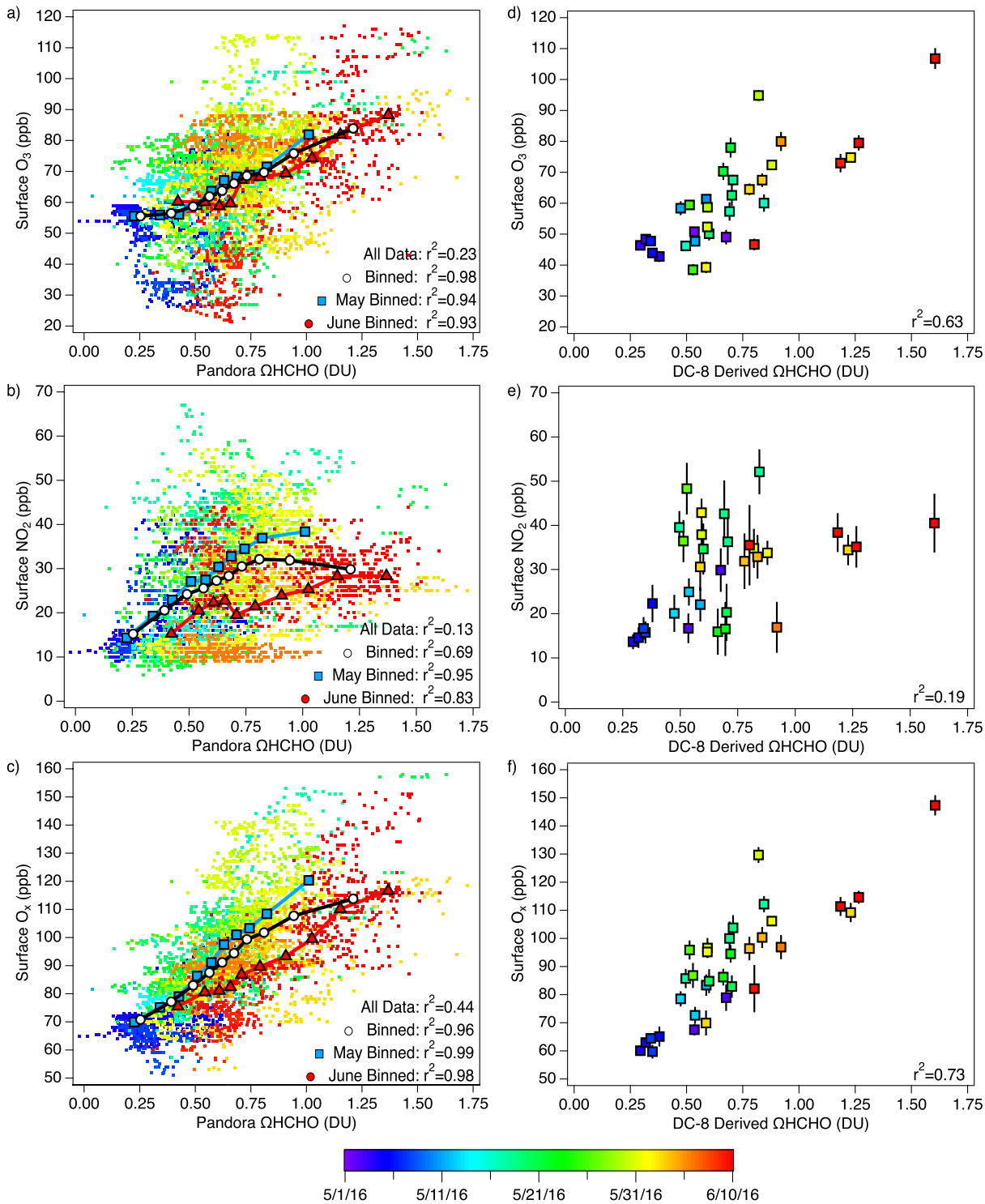

Figure 4. Pandora ΩHCHO versus surface (a) O_3, (b) NO_2, and (c) O_x at Olympic Park colored by date. Binned data show average O_3, NO_2, and O_x sorted by decile of ΩHCHO for all data (black circles), data in May (blue squares, n = 3,321), and data in June (red triangles, n = 1,616). ΩHCHO from DC-8 missed approaches versus surface (d) O_3, (e) NO_2, and (f) O_x colored by date.

During the LISTOS campaign, we identified both spatial and temporal relationships between ΩHCHO and surface ozone across nine consistently sampled sites. During KORUS-AQ, a strong temporal relationship with surface ozone was observed from ΩHCHO derived from the DC-8 aircraft and Pandora observations but not

from the airborne spectrometer. There was a similarly poor relationship for the subset of Pandora data limited to airborne spectrometer overpass times. This emphasizes the value of the large sampling density provided by Pandora for developing robust statistics of ΩHCHO–ozone for future studies of this relationship.

Titration of ozone by NO can impact the ΩHCHO–ozone relationship, which was evident in the observations made in Seoul. Aircraft in situ derived and Pandora ΩHCHO showed a stronger relationship with O_x than ozone. Observed NO_2 was approximately 27 ppb (29% of O_x) during KORUS-AQ compared to only 6 ppb (9% of O_x) during LISTOS. Pandora observations revealed that the slope of ΩHCHO–O_x decreased from May to June during KORUS-AQ. This was not due to decreased ozone production but likely a result of increased NO_2 oxidation to reservoir species such as PAN with rising temperatures and biogenic VOC emissions.

Different VOC precursors could result in a range in the ΩHCHO–ozone relationship. Schroeder et al. (2016) found a difference in the relationship between the ΩHCHO–ozone relationship in Maryland where biogenic emissions (i.e., isoprene) dominated the VOC budget compared to Houston where anthropogenic emissions were more important. In New York City, formaldehyde production has been shown to be driven by isoprene and alkenes (Lin et al., 2012). During KORUS-AQ, ozone production (and associated HCHO production) was dominated by aromatic VOCs, (∼50%), but with an important contribution from isoprene and alkenes (∼20% each; Schroeder et al., 2020). While the VOC mix was different for each campaign, the ΩHCHO–O_3 relationship was robust during both the biogenically dominated (LISTOS) and anthropogenically dominated (KORUS-AQ) campaigns. In contrast to Schroeder et al. (2016), campaign differences do not appear to preclude or affect a robust ΩHCHO–ozone relationship but shifts in ΩHCHO–O_x due to seasonality or different VOC mixtures motivate future investigations with longer-term data sets.

The EPA ozone NAAQS is in fact defined as a standard for both ozone and related photochemical oxidants (products of VOC oxidation in the presence of NO including NO_2, HCHO, PAN, and HNO_3; U.S. EPA, 1978, 2020). The greater sensitivity of ΩHCHO to O_x implies that this relationship could inform the spatial distribution of overall photochemical oxidants, not only ozone. As NO_x emissions are reduced due to policy measures, ozone will initially increase in VOC-limited conditions such as in Seoul, South Korea. In this case, ozone will become an increasing fraction of O_x and total photochemical oxidants.

The analysis of ΩHCHO–ozone from airborne and ground-based spectrometers during LISTOS and KORUS-AQ indicated that both averaged spatially and on a day-to-day basis, ΩHCHO corresponds to surface ozone and O_x. These relationships are not sufficiently robust to derive quantitative values for surface concentrations using ΩHCHO but instead show promise for future use to inform air quality monitoring strategies for ozone and related photochemical oxidants. The spatial relationship could be used as an indicator of potential ozone events and their regional extent that could be confirmed by surface monitors. In parts of the world where monitors may not be routinely operated, the temporal variability of ΩHCHO could be valuable for determining the frequency of extreme ozone events.

Future mapping of a region for this purpose requires sufficient temporal averaging to span the range of photochemical and meteorological conditions that impact air quality. The use of ΩHCHO from future geostationary satellites for this application is dependent on retrieval quality. The spatial range of ΩHCHO observed during LISTOS was 0.12 DU which was much smaller than the range observed from day to day (∼1 DU), challenging the ability to observe spatial gradients in ΩHCHO without high precision retrievals. The upcoming geostationary missions are evolving toward higher spatial/temporal resolution but with baseline precision requirements of 1×10^{16} molec cm^{-2} or 0.37 DU (Zoogman et al., 2017). The expected precision may be better with sufficient temporal averaging. With sufficient precision, the strong ΩHCHO–ozone relationship could be added to efforts combining satellite retrievals of multiple species with other ancillary measurements to infer to surface ozone concentrations (Requia et al., 2020; Zhang et al., 2018).

Pandora ΩHCHO data are just now becoming readily available. These data provide the best opportunity for further exploring the ΩHCHO–ozone (or O_x) relationship in more detail across the rapidly growing Pandonia Global Network (https://www.pandonia-global-network.org/; Szykman et al., 2019). Further uses include interpretation of ΩHCHO–ozone temporal variability and aircraft or satellite-based remote sensing of ΩHCHO. This could include investigating whether the ΩHCHO–ozone relationship shifts on days that exceed local ozone standards compared to average conditions (i.e., Koplitz et al., 2022). This unprecedented volume of ΩHCHO data

provides the unique opportunity to investigate ΩHCHO–ozone for diverse locations across the world, if colocated with ground-based ozone and ideally NO_2 and other photochemical oxidants.

Data Availability Statement

The LISTOS GCAS/GeoTASO aircraft and ground data (LISTOS Science Team, 2020) used for the calculation of ΩHCHO–O_x in the study are available at https://www-air.larc.nasa.gov/missions/listos/index.html. The KORUS-AQ GeoTASO, aircraft, and ground data (KORUS-AQ Science Team, 2019) used for the calculation of ΩHCHO–O_x are available at https://www-air.larc.nasa.gov/missions/korus-aq/index.html. The AirKorea NIER data are copyright by NIER (http://www.airkorea.or.kr). SLAMS data reported to the EPA AQS (U.S. EPA, 2019) are available at https://aqs.epa.gov/aqsweb/airdata/download_files.html.

Acknowledgments
The LISTOS airborne measurements would not have been possible without the support of the NASA Geostationary Coastal and Air Pollution Events (GEO-CAPE) mission study as well as the NASA Earth Science Division (ESD) Tropospheric Composition Program. We express gratitude to the entire LISTOS and KORUS-AQ science teams for their expertise, research, and measurement contributions toward the successful collaborative field study. We acknowledge Paul Wennberg for the use of his HNO_3 data from the CIT-CIMS, Greg Huey for the use of his PAN data from the GT-CIMS during KORUS-AQ, Sam Hall for the use of his photolysis frequency data from the CAFS instrument, and Bill Brune for the use of his OH data from the ATHOS instrument. The views expressed in this article are those of the authors and do not necessarily represent the views or policies of the U.S. Environmental Protection Agency. Any mention of trade names, manufacturers or products does not imply an endorsement by the United States Government or the U.S. Environmental Protection Agency. EPA and its employees do not endorse any commercial products, services, or enterprises.

References

Cooper, O. R., Parrish, D. D., Ziemke, J., Balashov, N. V., Cupeiro, M., Galbally, I. E., et al. (2014). Global distribution and trends of tropospheric ozone: An observation-based review. *Elementa: Science of the Anthropocene*, *2*, 000029. https://doi.org/10.12952/journal.elementa.000029

Costantino, L., Cuesta, J., Emili, E., Coman, A., Foret, G., Dufour, G., et al. (2017). Potential of multispectral synergism for observing ozone pollution by combining IASI-NG and UVNS measurements from the EPS-SG satellite. *Atmospheric Measurement Techniques*, *10*(4), 1281–1298. https://doi.org/10.5194/amt-10-1281-2017

Couillard, M. H., Schwab, M. J., Schwab, J., Lu, C.-H., Joseph, E., Stutsrim, B., et al. (2021). Vertical profiles of ozone concentrations in the lower troposphere downwind of New York City during LISTOS 2018–2019. *Journal of Geophysical Research: Atmospheres*, *126*, e2021JD035108. https://doi.org/10.1029/2021JD035108

Crawford, J. H., Ahn, J.-Y., Al-Saadi, J., Chang, L., Emmons, L. K., Kim, J., et al. (2021). The Korea–United States Air Quality (KORUS-AQ) field study. *Elementa: Science of the Anthropocene*, *9*(1), 00163. https://doi.org/10.1525/elementa.2020.00163

Duncan, B. N., Yoshida, Y., Olson, J. R., Sillman, S., Martin, R. V., Lamsal, L., et al. (2010). Application of OMI observations to a space-based indicator of NOx and VOC controls on surface ozone formation. *Atmospheric Environment*, *44*(18), 2213–2223. https://doi.org/10.1016/j.atmosenv.2010.03.010

Dunlea, E. J., Herndon, S. C., Nelson, D. D., Volkamer, R. M., San Martini, F., Sheehy, P. M., et al., (2007). Evaluation of nitrogen dioxide chemiluminescence monitors in a polluted urban environment. *Atmospheric Chemistry and Physics*, *7*, 2691–2704. https://doi.org/10.5194/acp-7-2691-2007

Fried, A., Walega, J., Weibring, P., Richter, D., Simpson, I. J., Blake, D. R., et al. (2020). Airborne formaldehyde and volatile organic compound measurements over the Daesan petrochemical complex on Korea's northwest coast during the Korea–United States Air Quality study. *Elementa: Science of the Anthropocene*, *8*(1), 121. https://doi.org/10.1525/elementa.2020.121

Gaudel, A., Cooper, O. R., Ancellet, G., Barret, B., Boynard, A., Burrows, J. P., et al. (2018). Tropospheric Ozone Assessment Report: Present-day distribution and trends of tropospheric ozone relevant to climate and global atmospheric chemistry model evaluation. *Elementa: Science of the Anthropocene*, *6*, 39. https://doi.org/10.1525/elementa.291

Gonzalez Abad, G., Souri, A. H., Bak, J., Chance, K., Flynn, L. E., Krotkov, N. A., et al. (2019). Five decades observing Earth's atmospheric trace gases using ultraviolet and visible backscatter solar radiation from space. *Journal of Quantitative Spectroscopy and Radiative Transfer*, *238*, 106478. https://doi.org/10.1016/j.jqsrt.2019.04.030

Ingmann, P., Veihelmann, B., Langen, J., Lamarre, D., Stark, H., & Courrèges-Lacoste, G. B. (2012). Requirements for the GMES Atmosphere Service and ESA's implementation concept: Sentinels-4/-5 and -5p. *Remote Sensing of Environment*, *120*, 58–69. https://doi.org/10.1016/j.rse.2012.01.023

Janz, S., Kowalewski, M. G., Lamsal, L., Nowlan, C., & Judd, L. (2019). Airborne hyperspectral trace gas sensors as testbeds for geostationary air quality missions. In S. P. Neeck, T. Kimura, & P. Martimort (Eds.), *Sensors, systems, and next-generation satellites XXIII* (p. 86). SPIE. https://doi.org/10.1117/12.2533765

Jin, X., Fiore, A., Boersma, K. F., Smedt, I. D., & Valin, L. (2020). Inferring changes in summertime surface ozone–NO_x–VOC chemistry over U.S. urban areas from two decades of satellite and ground-based observations. *Environmental Science & Technology*, *54*(11), 6518–6529. https://doi.org/10.1021/acs.est.9b07785

Jin, X., & Holloway, T. (2015). Spatial and temporal variability of ozone sensitivity over China observed from the Ozone Monitoring Instrument. *Journal of Geophysical Research: Atmospheres*, *120*, 7229–7246. https://doi.org/10.1002/2015JD023250

Judd, L. M., Al-Saadi, J. A., Szykman, J. J., Valin, L. C., Janz, S. J., Kowalewski, M. G., et al. (2020). Evaluating Sentinel-5P TROPOMI tropospheric NO_2 column densities with airborne and Pandora spectrometers near New York City and Long Island Sound. *Atmospheric Measurement Techniques*, *13*(11), 6113–6140. https://doi.org/10.5194/amt-13-6113-2020

Karambelas, A. (2020). LISTOS: Toward a better understanding of New York City's ozone pollution problem. *The Magazine for Environmental Managers*.

Kim, J., Jeong, U., Ahn, M.-H., Kim, J. H., Park, R. J., Lee, H., et al. (2020). New Era of air quality monitoring from space: Geostationary Environment Monitoring Spectrometer (GEMS). *Bulletin of the American Meteorological Society*, *101*(1), E1–E22. https://doi.org/10.1175/BAMS-D-18-0013.1

Koplitz, S., Simon, H., Henderson, B., Liljegren, J., Tonnesen, G., Whitehill, A., & Wells, B. (2022). Changes in ozone chemical sensitivity in the United States from 2007 to 2016. *ACS Environmental Au*, *2*, 206–222. https://doi.org/10.1021/acsenvironau.1c00029

KORUS-AQ Science Team. (2019). KORUS-AQ Data, [Dataset], NASA Langley Research Center. https://doi.org/10.5067/Suborbital/KORUSAQ/DATA01

Kowalewski, M. G., & Janz, S. J. (2014). Remote sensing capabilities of the GEO-CAPE Airborne Simulator. Paper presented at Proceedings of SPIE 9218, Earth Observing Systems XIX, 92181I (26 September 2014). https://doi.org/10.1117/12.2062058

Kwon, H.-A., Park, R. J., Oak, Y. J., Nowlan, C. R., Janz, S. J., Kowalewski, M. G., et al. (2021). Top-down estimates of anthropogenic VOC emissions in South Korea using formaldehyde vertical column densities from aircraft during the KORUS-AQ campaign. *Elementa: Science of the Anthropocene*, *9*(1), 00109. https://doi.org/10.1525/elementa.2021.00109

Leitch, J. W., Delker, T., Good, W., Ruppert, L., Murcray, F., Chance, K., et al. (2014). The GeoTASO airborne spectrometer project. Paper presented at Proceedings of SPIE 9218, Earth Observing Systems XIX, 92181H (2 October 2014). https://doi.org/10.1117/12.2063763

Lin, Y. C., Schwab, J. J., Demerjian, K. L., Bae, M.-S., Chen, W.-N., Sun, Y., et al. (2012). Summertime formaldehyde observations in New York City: Ambient levels, sources and its contribution to HOx radicals. *Journal of Geophysical Research*, *117*, D08305. https://doi.org/10.1029/2011JD016504

LISTOS Science Team. (2020). Long Island Sound Tropospheric Ozone Study. [Dataset]. NASA Langley Atmospheric Science Data Center DAAC. https://doi.org/10.5067/SUBORBITAL/LISTOS/DATA001

Martin, R. V., Fiore, A. M., & Van Donkelaar, A. (2004). Space-based diagnosis of surface ozone sensitivity to anthropogenic emissions. *Geophysical Research Letters*, *31*, L06120. https://doi.org/10.1029/2004GL019416

NESCAUM. (2017). Retrospective and future analysis of air quality in and downwind of New York city (White paper). Retrieved from https://www.nescaum.org/documents/nyc-metro-lis-ozone-whitepaper-final-201712.pdf

Requia, W. J., Di, Q., Silvern, R., Kelly, J. T., Koutrakis, P., Mickley, L. J., et al. (2020). An ensemble learning approach for estimating high spatiotemporal resolution of ground-level ozone in the Contiguous United States. *Environmental Science & Technology*, *54*(18), 11037–11047. https://doi.org/10.1021/acs.est.0c01791

Schroeder, J. R., Crawford, J. H., Ahn, J.-Y., Chang, L., Fried, A., Walega, J., et al. (2020). Observation-based modeling of ozone chemistry in the Seoul Metropolitan Area during the Korea–United States Air Quality Study (KORUS-AQ). *Elementa: Science of the Anthropocene*, *8*(1), 3. https://doi.org/10.1525/elementa.400

Schroeder, J. R., Crawford, J. H., Fried, A., Walega, J., Weinheimer, A., Wisthaler, A., et al. (2016). Formaldehyde column density measurements as a suitable pathway to estimate near-surface ozone tendencies from space. *Journal of Geophysical Research: Atmospheres*, *121*, 13088–13112. https://doi.org/10.1002/2016JD025419

Schroeder, J. R., Crawford, J. H., Fried, A., Walega, J., Weinheimer, A., Wisthaler, A., et al. (2017). New insights into the column CH_2O/NO_2 ratio as an indicator of near-surface ozone sensitivity. *Journal of Geophysical Research: Atmospheres*, *122*, 8885–8907. https://doi.org/10.1002/2017JD026781

Spinei, E., Tiefengraber, M., Müller, M., Gebetsberger, M., Cede, A., Valin, L., et al. (2021). Effect of polyoxymethylene (POM-H Delrin) off-gassing within the Pandora head sensor on direct-sun and multi-axis formaldehyde column measurements in 2016–2019. *Atmospheric Measurement Techniques*, *14*(1), 647–663. https://doi.org/10.5194/amt-14-647-2021

Spinei, E., Whitehill, A., Fried, A., Tiefengraber, M., Knepp, T. N., Herndon, S., et al. (2018). The first evaluation of formaldehyde column observations by improved Pandora spectrometers during the KORUS-AQ field study. *Atmospheric Measurement Techniques*, *11*(9), 4943–4961. https://doi.org/10.5194/amt-11-4943-2018

Szykman, J., Swap, R. J., Lefer, B., Valin, L., Lee, S. C., Fioletov, V., et al. (2019). Pandora: Connecting in-situ and satellite monitoring in support of the Canada–U.S. air quality agreement. *The Magazine for Environmental Managers*. Retrieved from https://pubs.awma.org/flip/EM-June-2019/szykman.pdf

Tonnesen, G. S., & Dennis, R. L. (2000). Analysis of radical propagation efficiency to assess O_3 sensitivity to hydrocarbons and NOx: 2. Long-Lived species as indicators of O_3 concentration sensitivity. *Journal of Geophysical Research*, *105*, 9227–9241. https://doi.org/10.1029/1999JD900372

U.S. EPA. (1978). *Air quality criteria for ozone and other photochemical oxidants* (EPA Report EPA/600/8-78/004). U.S. EPA. Retrieved from http://nepis.epa.gov/exe/ZyPURL.cgi?Dockey=200089CW.txt

U.S. EPA. (2019). Air quality system data mart (internet database). Retrieved from https://www.epa.gov/outdoor-air-quality-data

U.S. EPA. (2020). *Integrated science assessment (ISA) for ozone and related photochemical oxidants (final report, Apr 2020)* (EPA/600/R-20/012). U.S. Environmental Protection Agency.

U.S. EPA. (2021). 8-Hour ozone (2015) designated area design values. Retrieved from https://www3.epa.gov/airquality/greenbook/jdtc.html

Zhang, Y., Wang, Y., Crawford, J., Cheng, Y., & Li, J. (2018). Improve observation-based ground-level ozone spatial distribution by compositing satellite and surface observations: A simulation experiment. *Atmospheric Environment*, *180*, 226–233. https://doi.org/10.1016/j.atmosenv.2018.02.044

Zoogman, P., Liu, X., Suleiman, R. M., Pennington, W. F., Flittner, D. E., Al-Saadi, J. A., et al. (2017). Tropospheric emissions: Monitoring of pollution (TEMPO). *Journal of Quantitative Spectroscopy and Radiative Transfer*, *186*, 17–39. https://doi.org/10.1016/j.jqsrt.2016.05.008

References From the Supporting Information

Brion, J., Chakir, A., Daumont, D., Malicet, J., & Parisse, C. (1993). High-resolution laboratory absorption cross section of O_3. Temperature effect. *Chemical Physics Letters*, *213*, 610–612. https://doi.org/10.1016/0009-2614(93)89169-I

Chance, K., Kurosu, T. P., & Sioris, C. E. (2005). Undersampling correction for array detector-based satellite spectrometers. *Applied Optics*, *44*, 1296. https://doi.org/10.1364/AO.44.001296

Chance, K., & Orphal, J. (2011). Revised ultraviolet absorption cross sections of H_2CO for the HITRAN database. *Journal of Quantitative Spectroscopy and Radiative Transfer*, *112*, 1509–1510. https://doi.org/10.1016/j.jqsrt.2011.02.002

Chance, K. V., & Spurr, R. J. D. (1997). Ring effect studies: Rayleigh scattering, including molecular parameters for rotational Raman scattering, and the Fraunhofer spectrum. *Applied Optics*, *36*, 5224. https://doi.org/10.1364/AO.36.005224

Goldberg, D. L., Saide, P. E., Lamsal, L. N., de Foy, B., Lu, Z., Woo, J.-H., et al. (2019). A top-down assessment using OMI NO_2 suggests an underestimate in the NOx emissions inventory in Seoul, South Korea, during KORUS-AQ. *Atmospheric Chemistry and Physics*, *19*, 1801–1818. https://doi.org/10.5194/acp-19-1801-2019

Lorente, A., Folkert Boersma, K., Yu, H., Dörner, S., Hilboll, A., Richter, A., et al. (2017). Structural uncertainty in air mass factor calculation for NO_2 and HCHO satellite retrievals. *Atmospheric Measurement Techniques*, *10*, 759–782. https://doi.org/10.5194/amt-10-759-2017

Lucht, W., Schaaf, C. B., & Strahler, A. H. (2000). An algorithm for the retrieval of albedo from space using semiempirical BRDF models. *IEEE Transactions on Geoscience and Remote Sensing*, *38*, 977–998. https://doi.org/10.1109/36.841980

Meller, R., & Moortgat, G. K. (2000). Temperature dependence of the absorption cross sections of formaldehyde between 223 and 323 K in the wavelength range 225–375 nm. *Journal of Geophysical Research*, *105*, 7089–7101. https://doi.org/10.1029/1999JD901074

Nowlan, C. R., Liu, X., Janz, S. J., Kowalewski, M. G., Chance, K., Follette-Cook, M. B., et al. (2018). Nitrogen dioxide and formaldehyde measurements from the GEOstationary Coastal and Air Pollution Events (GEO-CAPE) Airborne Simulator over Houston, Texas. *Atmospheric Measurement Techniques*, *11*, 5941–5964. https://doi.org/10.5194/amt-11-5941-2018

Schaaf, C., & Wang, Z. (2015). MCD43A1 MODIS/Terra + Aqua BRDF/Albedo model parameters daily L3 global—500m V006. https://doi.org/10.5067/MODIS/MCD43A1.006

Serdyuchenko, A., Gorshelev, V., Weber, M., Chehade, W., & Burrows, J. P. (2014). High spectral resolution ozone absorption cross-sections—Part 2: Temperature dependence. *Atmospheric Measurement Techniques*, *7*, 625–636. https://doi.org/10.5194/amt-7-625-2014

Thalman, R., & Volkamer, R. (2013). Temperature dependent absorption cross-sections of O_2–O_2 collision pairs between 340 and 630 nm and at atmospherically relevant pressure. *Physical Chemistry Chemical Physics*, *15*, 15371. https://doi.org/10.1039/c3cp50968k

Vandaele, A. C., Hermans, C., Simon, P. C., Carleer, M., Colin, R., Fally, S., et al. (1998). Measurements of the NO_2 absorption cross-section from 42 000 cm^{-1} to 10 000 cm^{-1} (238–1000 nm) at 220 K and 294 K. *Journal of Quantitative Spectroscopy and Radiative Transfer*, *59*, 171–184. https://doi.org/10.1016/S0022-4073(97)00168-4

Wilmouth, D. M., Hanisco, T. F., Donahue, N. M., & Anderson, J. G. (1999). Fourier transform ultraviolet spectroscopy of the A $^2\Pi_{3/2} \leftarrow$ X $^2\Pi_{3/2}$ transition of BrO. *Journal of Physical Chemistry A*, *103*, 8935–8945. https://doi.org/10.1021/jp991651o

Zoogman, P., Liu, X., Chance, K., Sun, Q., Schaaf, C., Mahr, T., & Wagner, T. (2016). A climatology of visible surface reflectance spectra. *Journal of Quantitative Spectroscopy and Radiative Transfer*, *180*, 39–46. https://doi.org/10.1016/j.jqsrt.2016.04.003